Kennett, J.P., Baldauf, J.G., and Lyle, M. (Eds.), 1995
Proceedings of the Ocean Drilling Program, Scientific Results, Vol. 146 (Pt. 2)

7. CLAY AND BULK MINERALOGY OF LATE QUATERNARY SEDIMENTS AT SITE 893, SANTA BARBARA BASIN[1]

Ruediger Stein[2]

ABSTRACT

To characterize and quantify the siliciclastic sediment fraction and its change through late Quaternary times, sediments of Ocean Drilling Program Site 893 were analyzed for their clay and bulk mineralogical composition using X-ray diffraction (XRD) techniques. Throughout the entire sediment sequence, smectite (40%–68%) and illite (25%–44%) are the dominant clay minerals, whereas kaolinite (5%–10%) and chlorite (3%–9%) are only of secondary importance. Quartz contents vary between 12%–25%; quartz fluxes range from 10 to 40 g/cm^{-2}k.y.$^{-1}$. The Santa Clara River appears to be a major sediment source over the past 160,000 years. During glacial intervals of lowered sea level, a direct sediment transport from the shelf/slope probably became more important. The sandy material is characterized by very high quartz content (55%) and significantly higher k-feldspar/plagioclase ratios. Based on the still-limited data base, short-term fluctuations in clay-mineral composition and quartz content occur, suggesting climate-triggered changes in the terrigenous sediment supply. (Eolian) quartz flux was significantly increased during glacial stages 2, 5d, and near the stage 5/6 boundary. Future high-resolution studies on clay and bulk mineralogy are necessary to prove these preliminary interpretations.

INTRODUCTION

In the past, paleoenvironmental studies of Quaternary sediments from the Santa Barbara Basin, California, were restricted to the Holocene time interval. Numerous high-resolution sedimentological, geochemical, and micropaleontological studies demonstrated that the sedimentation in the basin is mainly controlled by terrigenous sediment supply, surface-water productivity, bacterial activity, and oxygenation of bottom water (e.g., Soutar and Crill, 1977; Heusser, 1978; Pisias, 1978; Dunbar, 1983; Thornton, 1984; Lange et al., 1990; Reimers et al., 1990; Baumgartner et al., 1991; Kennedy and Brassell, 1992; Schimmelmann et al., 1992). The sedimentary sequence of Ocean Drilling Program Site 893 presents the unique possibility to extend the investigation of paleoenvironmental change in the Santa Barbara Basin to pre-Holocene times.

Site 893 was drilled at 34° 17.25′N, 120° 02.2′W in the central part of the Santa Barbara Basin, 20 km south of the Santa Barbara coastline at a water depth of 576.5 m (Fig. 1). A 196.5-m-thick sequence of upper Quaternary terrigenous silt and clay with variable contents of calcareous nannofossils and diatoms was recovered (Kennett, Baldauf, et al., 1994). Based on oxygen-isotope stratigraphy, the sequence represents isotope stages 1 to 6, the last about 160,000 yr. ago (Ingram and Kennett, this volume). The upper 24.25 mbsf (meters below seafloor) (approximately corresponding to oxygen-isotope stage 1) and the interval from 131.0 to 145.5 mbsf (approximately corresponding to warm oxygen-isotope interstadial 5e) are characterized by variably preserved laminations throughout and thin to medium (1–15 cm) gray beds of interbedded clayey silt and silty clay. In the other intervals of the sedimentary sequence of Site 893, laminations are less pronounced or absent. Four medium to thick beds of sand occur between 56.5 and 64.7 mbsf, and a 2.5-m-thick sand bed occurs at 114.4–116.9 mbsf (Kennett, Baldauf, et al., 1994).

The major purposes of this pilot study on clay and bulk mineralogy are (1) to characterize and quantify the siliciclastic sediment fraction and its change through time, and (2) to identify different sources of Santa Barbara sediments. During times of lowered sea level, the processes controlling the sedimentation in the Santa Barbara Basin probably have changed significantly from high sea-level stand because of changes in climate-triggered fluvial discharge, oceanic-circulation patterns, and downslope transport of coarse-grained shelf sediments.

MODERN SEDIMENTARY PROCESSES IN THE SANTA BARBARA BASIN

Based on studies of surface sediments and piston cores, the major processes controlling the terrigenous sediment supply in the Santa Barbara Basin are river discharge, suspension transport by oceanic currents, turbidity-current transport, and mass movements at the continental slope (Fleischer, 1972; Soutar and Crill, 1977; Thornton, 1984). Seasonal variation in river discharge is one of the factors causing the varve-like sediments dominant in the Holocene sedimentary sequence. The varves are well preserved because of the absence of bioturbation due to sub-/anoxic bottom-water conditions (Hülsemann and Emery, 1961; Sholkovitz and Gieskes, 1971; Soutar and Crill, 1977).

During major flood events, huge amounts of suspended matter are transported to the shelf by the Santa Clara and the Ventura rivers (Fig. 1; Drake et al., 1972; Thornton, 1984). Part of the material is deposited on the shelf; part of the suspension is further transported into the deep basin via currents. The importance of the interaction between river discharge and westward transport by the Anacapa Current as sources for fine-grained material in the Santa Barbara Basin becomes obvious in the distribution of terrigenous silt in surface sediments (Fig. 1; Thornton, 1984). A second source for silt-sized material appears to be in the west, controlled by the southeastward-

[1] Kennett, J.P., Baldauf, J.G., and Lyle, M. (Eds.), 1995. *Proc. ODP, Sci. Results*, Vol. 146 (Pt. 2): College Station, TX (Ocean Drilling Program).

[2] Alfred-Wegener-Institute for Polar and Marine Research, Columbusstrasse, 27568 Bremerhaven, Federal Republic of Germany.

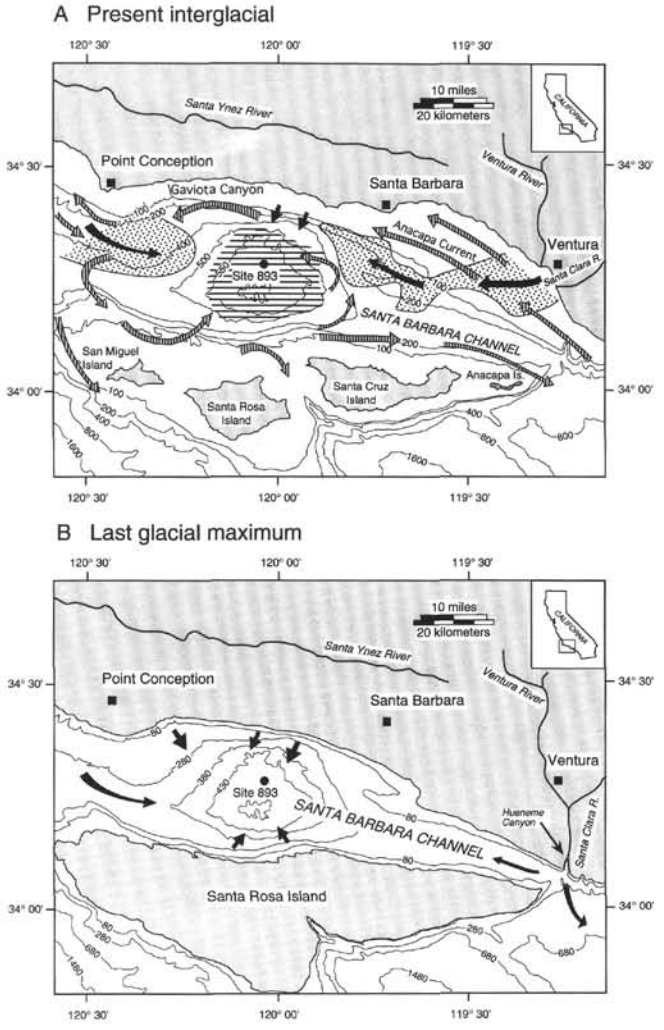

Figure 1. Map of the Santa Barbara Basin and location of Site 893 (from Kennett, Baldauf, et al., 1994). **A.** Modern (interglacial) situation. **B.** Last glacial maximum situation, assuming a glacial sea-level fall of 120 m (from Kennett, Baldauf, et al., 1994). Dotted fields mark maxima in occurrence of silt-sized material in surface sediments; hatched area marks occurrence of gray beds (from Thornton, 1984). Hatched arrows indicate surface currents (Hickey, 1992; Kennett, Baldauf, et al., 1994). Black arrows indicate major pathways of terrigenous material. Bathymetry is shown in meters.

flowing California Current (Fig. 1). These processes are probably the dominant mechanism forming the thin homogeneous gray layers or beds (flood deposits) that commonly occur in the Holocene sedimentary sequences in the central Santa Barbara Basin. In comparison to the normal sedimentation, the gray layers are significantly depleted in biogenic carbonate (Table 1), interpreted as rapid deposition from shelf or river sediments (Fleischer, 1972). Because of the absence of both sand-sized material and sedimentary structures, a turbidity-current origin is rather unlikely for these thin gray layers. The thicker gray beds (>2 cm thick), on the other hand, show some internal structures such as lamination and upward-fining, which are interpreted as distal mud turbidites with an upper slope origin (Thornton, 1984).

The mineral compositions of the dominant olive silty clay to clayey silt lithology and the gray beds are similar. Smectite (montmorillonite) and illite are the predominant clay minerals; kaolinite and chlorite are of minor importance (Table 1). Furthermore, these values also are similar to clay mineral data from the Santa Clara River sediments (Table 1), suggesting that the Santa Clara River is the most probable source of the terrigenous material of both lithologies in the central Santa Barbara Basin (Fleischer, 1972).

METHODS

To determine the amounts of sand, silt, and clay fractions, the 47 samples investigated in this pilot study were first wet-sieved through a 63-μm sieve. From the <63-μm fraction, the silt (2–63 μm) and clay (<2 μm) fractions were separated using settling tubes ("Atterberg method"; Müller, 1967).

Clay minerals have been determined from the clay (<2 μm) fraction using X-ray diffraction technique (XRD). After the addition of 1 mL of 1% MoS_2 suspension as an internal standard to a 40-mg clay sample, the homogenized clay sample was sucked onto a cellulose nitrate filter (0.15 μm pore width) under vacuum conditions to produce a texturally oriented sample (Lange, 1982). The sample was measured by means of a Philips PW1700 XRD system with cobalt Ka-radiation. The measurements were performed on untreated samples from 2° to 18° 2θ and glycolated (18 hr at 60°C) samples from 2° to 40° 2θ in 0.02° steps for 2 seconds at each step. For separation of the kaolinite/chlorite 7-Å peak, an additional scan was performed in 0.005° steps for 2 sec at each step between 28° and 30.5° 2θ to determine the 3.54-Å peak of chlorite and the 3.58-Å peak of kaolinite (Biscaye, 1965). Using a graphic evaluation program ("MacDiff"; Petschick et al., 1995) peak areas were determined and multiplied by "Biscaye factors" (Biscaye, 1965): smectite = 17 Å glycolated, (×1); illite = 10 Å (×4), and chlorite + kaolinite = 7 Å (×2). The 7-Å peak was separated into a kaolinite and chlorite proportion using the heights of the kaolinite peak (002-order peak; 3.58 Å) and the chlorite peak (004-order peak; 3.54 Å) (Fig. 2). The sum of the weighted peak areas accounts for 100% of the clay minerals of the <2-μm sample. Smectite/illite ratios were calculated using the smectite and illite percentage values.

For bulk mineralogy determinations, 15% corundum was added as an internal standard to the ground bulk sample. Then, XRD measurements were performed on randomly oriented, pressed powder slides from 2° to 62° 2θ at 0.03° steps per second, by means of the Philips PW1700 system. In this paper, quartz contents (in percent of bulk sediment) and quartz/feldspar ratios are given. The accuracy of the quartz measurement is about ±5% (for the method of quantitative and qualitative determination of bulk mineralogy see Emmermann et al., 1989; Dersch, 1994).

Mass accumulation rates (MAR) were calculated according to van Andel et al. (1975):

$$MAR = LSR \cdot (WBD - 1.026 \cdot (PO/100)) = LSR \cdot DD,$$

where LSR = linear sedimentation rate (cm/k.y.), WBD = wet bulk density (g/cm^3), DD = dry density (g/cm^3), and PO = porosity (%). The linear sedimentation rates are based on AMS ^{14}C chronology and oxygen-isotope stratigraphy (Ingram and Kennett, this volume). Physical properties are based on shipboard measurements (see Kennett, Baldauf, et al., 1994).

RESULTS

Grain Size Data (Sand-silt-clay Contents)

Clayey silt to silty clay is clearly the dominant lithology at Site 893 (Figs. 3A and 4; Table 2). Silt and clay vary from 37%–72% and

Table 1. Concentrations of sand, carbonate, quartz, and clay-mineral composition of sediments.

	% of bulk sediment			% of clay fraction					
	Sand	$CaCO_3$	Quartz	Montmor. (17A glyc.)	Illite (10 A)	Kaol. + Chlo. (7 A)	Kaolinite	Chlorite	Vermiculite
Modern rivers and canyons									
Santa Clara River			19	51	34	15	15	0	0
Ventura River		2.6	30	30	53	13	10	2	4
Santa Ynez River			15	24	52	17	14	3	7
Gaviota Canyon			29	37	47	11	8	3	5
Surface sediment and piston core data									
Olive silt-clay	0.65	9.8	21	47	36	14	10	3	4
Gray beds	0.06	2.5	22	48	38	12	10	2	3
Site 893 (mean values)									
olive clayey silt/silty clay	1.5	6.5 (8)	20	55	32	1376			
gray bed	0	2.8	22	44	44	12	5	7	
sand bed	86.5	2.0	55	42	40	18	9	9	

Notes: Olive silt/clay and gray bed lithologies in piston cores from the Santa Barbara Basin; Site 893 river, canyon, and piston-core data from Fleischer (1972); data base for mean carbonate values of Site 893 from Stein and Rack (this vol.); carbonate value in bracket indicates mean Holocene value.

34%–65%, respectively. There is no significant difference between the predominant olive lithology and the gray beds. No major long-term change in grain-size variation is obvious.

Between 58 and 69 mbsf and at about 109 mbsf sand beds and sandy-silt layers occur. The sand percentages reach values of 25%–87% (Figs. 3A, 4; Table 2).

Clay Mineralogy

Throughout the entire sediment sequence of Site 893, smectite and illite are the dominant clay minerals ranging from 40%–68% and 25%–44%, respectively (Figs. 3B and 4; Table 2). Kaolinite and chlorite are of secondary importance, reaching values of 5%–10% and 3%–9%, respectively. Mixed-layer minerals mainly consisting of ethylene glycol-expandable layers and detectable as shoulders or broad reflections between 10.5 Å and 14 Å (non-regular illite-smectite mixed-layer components), do not occur in detectable amounts. Over the last 160,000 years no major change in clay-mineral composition was recorded. There appears to be a slight increase (decrease) in smectite (illite) in the upper ~85 mbsf (i.e., during the last 60,000 years), resulting in an increase of the smectite/illite ratios from values of 1.2–1.8 to values of 1.5–2.5 (Figs. 5 and 4). Furthermore, a weak cyclicity in clay-mineral variations (smectite, illite) is indicated, which has, however, to be proved by a more densely-sampled (high-resolution) record.

A few clay-mineral measurements were performed on samples from gray silt and sand beds. These beds display reduced smectite and increased illite values (Figs. 2 and 5). In the one sample from a gray bed, the kaolinite/chlorite ratio is <1 (Fig. 2), whereas in all other samples from the dominant olive-colored lithology the kaolinite/chlorite ratio is >1 (Table 2). In the sand layer, also the maximum contents of kaolinite and chlorite were measured (Fig. 5).

Vermiculite, determined in piston cores from the Santa Barbara Basin (Table 1; Fleischer, 1972), could not be identified. In the smectite-rich and chlorite-containing sediments of the Santa Barbara Basin it appears to be very problematic to determine small amounts of vermiculite precisely because of the overlap of the major peaks used to identify the minerals.

Bulk Mineralogy

In the dominant clayey-silt to silty-clay lithologies, quartz contents vary between 10 and 25%, showing no long-term change (Fig. 6). In the quartz as well as in the quartz/feldspar and plagioclase/k-feldspar ratios, however, short-term cyclic variations are obvious. Quartz minima appear to occur during the warm interstadials 5a, 5c, and 5e and during the Holocene (Fig. 6). In general, plagioclase dominates over k-feldspar (Figs. 6, 7, and 8; Table 2). The carbonate is exclusively (biogenic) calcite (cf., Fig. 8); other carbonate minerals do not occur in detectable amounts.

The sand beds are distinctly enriched in quartz (up to 55%) and k-feldspar (i.e., the k-feldspar/plagioclase ratio reaches a value of up to 0.9), whereas the gray bed displays no significant difference in these variables in comparison to the olive lithology (Figs. 6, 7, and 8; Table 2). The main difference between the diffractograms of the olive clayey silt (Fig. 8A) and the gray bed (Fig. 8B) is reflected in the biogenic calcite peaks, showing relatively high values in the former and very low values in the latter.

DISCUSSION

Records on the mineralogical composition and grain-size distribution determined in marine sediment cores can give important information about different source areas and transport mechanisms of the terrigenous material as well as the climate of the source area and their changes through time, as shown in numerous studies from different parts of the world ocean (e.g., Biscaye, 1965; Fleischer, 1972; Sarnthein et al., 1981; Lange, 1982; Janecek and Rea, 1983; Stein and Robert, 1985; Cremer et al., 1989; Chamley, 1989, Leinen and Sarnthein, 1989; Dersch and Stein, 1994; Stein et al., 1994).

Mineralogy and Source of Terrigenous Matter

In general, the clay-mineral compositions as well as the quartz contents of the dominant lithologies at Site 893 are similar to those described for near-surface sediments from piston cores. Smectite (mean 55%) dominates over illite (mean 32%); kaolinite plus chlorite do not exceed 15%. Quartz contents are about 20% (Tables 1 and 2). The differences in the kaolinite and chlorite concentrations should not be over-interpreted because the separation of the kaolinite/chlorite proportions becomes less precise if both clay minerals only occur in minor amounts (cf., Fig. 2). I do not follow the more extensive interpretation of the chlorite (and vermiculite; see above) data performed by Fleischer (1972), who distinguished changes in clay-mineral source based on changes in chlorite and vermiculite contents of 1%–2%.

Both clay-mineral composition and quartz content at Site 893 are close to the corresponding data from the Santa Clara River. This may indicate that this river—as today (see above)—was also a major sediment source for the pre-Holocene terrigenous sediments in the Santa Barbara Basin. During times of increased illite content (and decreased smectite content), on the other hand, the terrigenous sediment supply from the Ventura River and/or from the continental slope

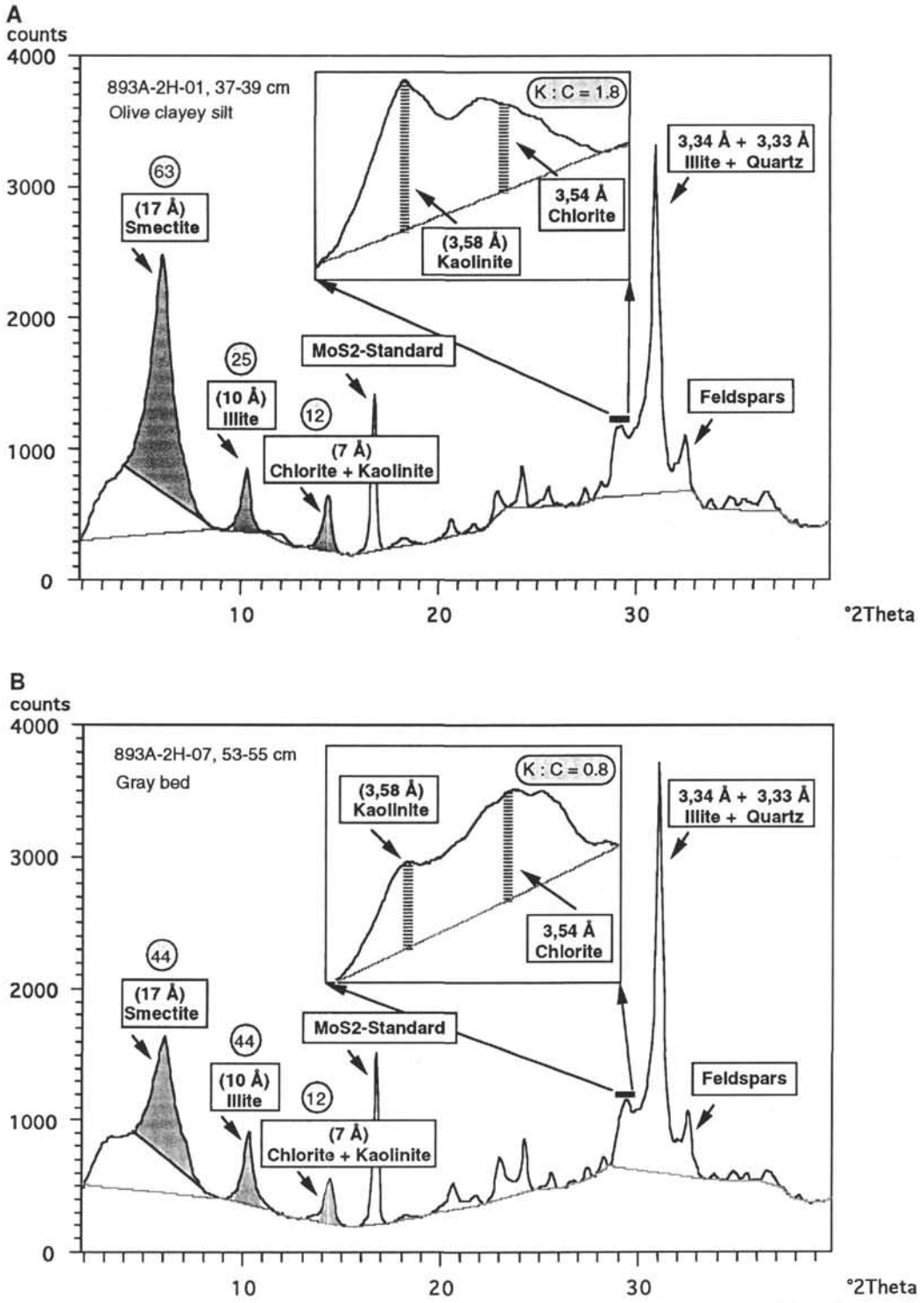

Figure 2. Diffractograms from samples of **(A)** olive clayey silt and **(B)** gray bed, indicating differences and similarities between the two lithologies and showing the principle of clay-mineral evaluation used in this study. Peak areas of the major clay minerals used for evaluation of percentage values are marked in gray. Percentage values are presented as circled numbers. K:C indicates kaolinite/chlorite ratio of the 3.58-Å/3.54-Å peaks (cf. Table 2).

(e.g., via the Gaviota Canyon) was probably more important than today (Table 1).

In comparison with the normal olive lithology, the gray-bed mineralogy is characterized by higher illite and distinctly lower (biogenic) calcite values. Based on piston-core data, the origin of the thin gray beds is related to major flood events (Fleischer, 1972; Thornton, 1984). This suggests that during these flood events the relative proportion of sediment input via the Ventura River was significantly increased compared to the input via the Santa Clara River. These gray layers are almost restricted to the interglacial stages 1 and 5e (Kennett, Baldauf, et al., 1994), that is, to times of high sea level. Because of the absence of the gray layers/beds during oxygen-isotope stages

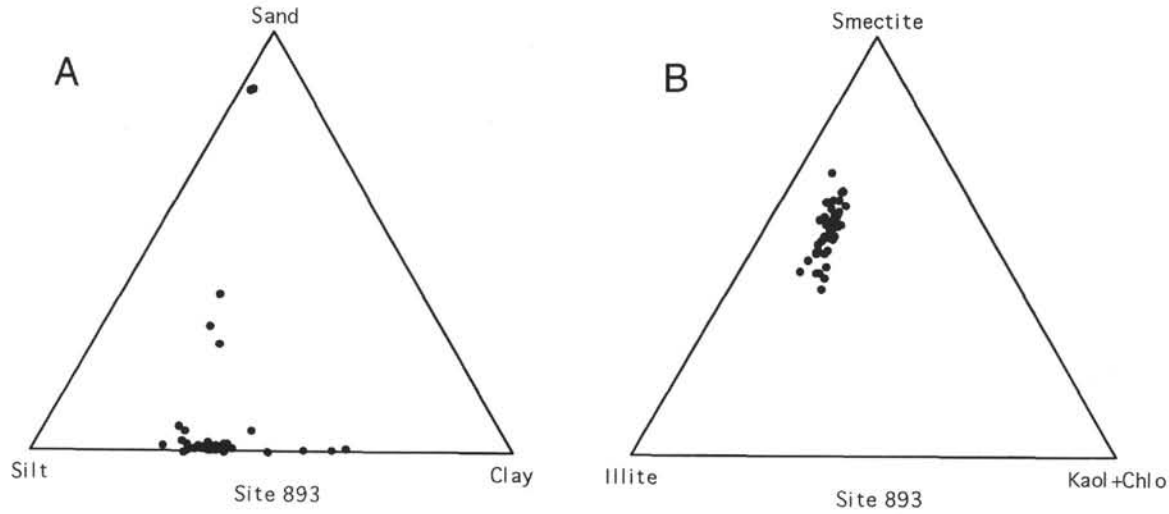

Figure 3. (**A**) Grain-size data distribution (sand-silt-clay) and (**B**) clay mineral distribution (smectite, illite, kaolinite + chlorite) at Site 893, plotted as triangle diagrams.

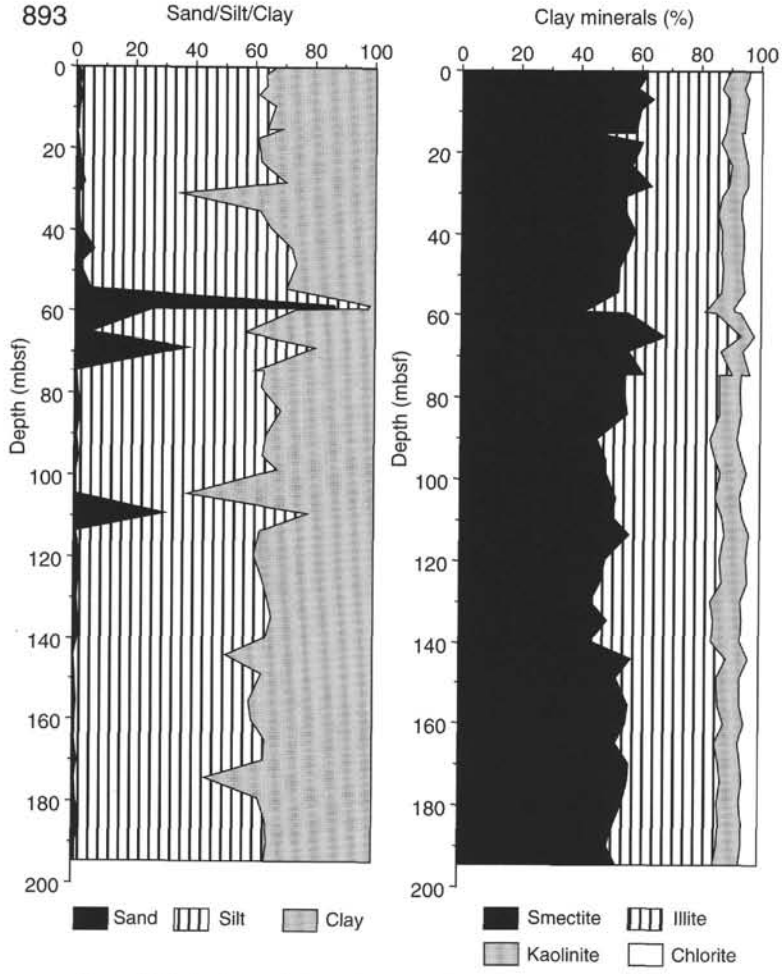

Figure 4. Grain-size and clay-mineral distributions vs. depth at Site 893.

2, 3, 5d, and 6, major flood events probably did not occur at those times. Because thin sand layers are still preserved in the more homogenous and bioturbated sections of these time intervals, the absence of gray layers cannot be explained by reduced preservation because of bioturbation. The sandy beds, on the other hand, which are concentrated in oxygen-isotopes stages 2, 3, 5d, and 6 (Kennett, Baldauf, et al., 1994), may have been produced by down-slope transport during times of lowered sea level. High amounts of sand-sized quartz and a distinctly higher content of k-feldspar (Fig. 6; Tables 1 and 2) point to a different source than do the other lithologies, such as the shelf/upper slope area and a transport through the Gaviota Canyon. During these times of lowered sea level, the terrigenous sediment supply into

the Santa Barbara Basin via the Santa Clara and Ventura rivers might have been significantly reduced because large amounts of the river load were probably bypassed though the Hueneme Canyon toward the east (Fig. 1B).

Variations in Concentration and Flux of Quartz Through Time

According to the record of quartz concentrations through the past 160,000 years, minima appear to correlate with warm interstadials 5a, 5c, and 5e and the Holocene, whereas during oxygen stages 6 and 4 to 2, quartz values were increased (Fig. 6). There is no clear correlation between quartz and specific clay mineral composition. In order to estimate changes in quartz flux, the percentage values were transferred into mass accumulation rates (Fig. 9; Table 3). Because mean sedimentation rates were used, single quartz peaks should not be over-interpreted. Instead, the general trend is important. In general, the quartz accumulation rates vary between 10 and 40 $g/cm^{-2}k.y.^{-1}$. Flux maxima occur during glacial stage 2, stage 5d, and near the stage 5/6 boundary.

This increased supply of quartz appears to correlate with times of lowered sea level, suggesting intensified bypass of suspended matter from the shelf/slope into the deep basin. A significant part of the silt-sized quartz may also have an eolian origin. Today, the haze and the dust distribution off the southwest coast of the United States and Baja California in Mexico display a significant maximum in spring and summer. The sources of these aerosols are the North American deserts which, thus, are thought to be a potential source area of the quartz-rich sediments in the eastern North Pacific Ocean (Prospero, 1981; Pye, 1987). On a global scale, during the glacials the atmospheric circulation was increased because of increased pole-equator-temperature gradient, and the major deserts were extended, resulting in a distinct increase in eolian flux to the open ocean (e.g., Sarnthein et al., 1981; Janecek and Rea, 1983; Leinen and Sarnthein, 1989, and further references therein; Dersch and Stein, 1994).

Looking at the changes in composition and flux of terrigenous matter through time, only preliminary interpretations are presented here. That means, these interpretations are based on a still-limited data set and must be substantiated by further analyses. For a more detailed discussion of the short-term fluctuations of terrigenous input on the Milankovitch scale as well as higher frequencies, and their relationship to climate change, a high-resolution study on clay and bulk mineralogy is needed.

CONCLUSIONS

The preliminary results of this study on clay and bulk mineralogy of sediments from Site 893 can be summarized as follows:

1. The terrigenous clayey silt to silty clays of Site 893 are characterized by a clear predominance of smectite (mean 55%) and illite (mean 32%); kaolinite plus chlorite do not exceed 15%. Quartz contents vary between 12%–25%, with the higher values more typical for the glacial and cold interstadials. Quartz fluxes vary between 10 and 40 $g/cm^{-2}/k.y.^{-1}$.
2. Both the clay-mineral composition and quartz content at Site 893 are similar to the mineralogy of the Santa Clara River, suggesting that this river was also a major sediment source for the pre-Holocene Santa Barbara Basin sediments.
3. Based on a still limited data set, the mineralogy of the gray beds and sand beds points to different sediment sources, such as the Ventura River and/or the shelf/slope area.
4. Short-term fluctuations in clay-mineral composition and quartz appear to occur and may suggest climate-triggered changes in terrigenous sediment supply. Maxima in quartz flux during glacial stage 2, stage 5d, and near the stage 5/6 boundary may indicate intensified bypass of suspended matter from the shelf/slope into the deep basin and increased eolian input. A more high-resolution study on bulk and clay mineralogy should follow to prove this hypothesis.

ACKNOWLEDGMENTS

I thank M. Apel, C. Vogt, and M. Wahsner for technical assistance and data discussion. The reviews by J.R. Boles and C. Robert are gratefully acknowledged. This is contribution No. 787 of the Alfred-Wegener-Institute for Polar and Marine Research, Bremerhaven, Federal Republic of Germany.

REFERENCES

Baumgartner, T.R., Ferreira-Bartrina, V., Cowen, J., and Soutar, A., 1991. Reconstruction of a twentieth century varve chronology from the central Gulf of California. *In* Dauphin, J.P., and Simoneit, B.R.T. (Eds.), *The Gulf and Peninsular Province of the Californias.* AAPG Mem., 47:603–616.

Biscaye, P.E., 1965. Mineralogy and sedimentation of recent deep-sea clays in the Atlantic Ocean and adjacent seas and oceans. *Geol. Soc. Am. Bull.,* 76:803–832.

Chamley, H., 1989. *Clay Sedimentology:* Berlin (Springer-Verlag).

Cremer, M., Maillet, N., and Latouche, C., 1989. Analysis of sedimentary facies and clay mineralogy of the Neogene-Quaternary sediments in ODP Site 646, Labrador Sea. *In* Srivastava, S.P., Arthur, M.A., Clement, B., et al., *Proc. ODP, Sci. Results,* 105: College Station, TX (Ocean Drilling Program), 71–81.

Dersch, M., 1994. Zur Klimaentwicklung in Ostasien während der letzten 5 Millionen Jahre: Terrigener Sedimenteintrag in die Japan See (ODP-Ausfahrt 128). Berichte Fachbereich Geowissenschaften, Universität Bremen, 49.

Dersch, M., and Stein, R., 1994. Late Cenozoic records of eolian quartz flux in the Sea of Japan (ODP-Leg 128 Sites 798 and 799) and paleoclimate in Asia. *Palaeogeogr., Palaeoclimatol., Palaeoecol.,* 108:523–535.

Drake, D.E., Kolpack, R.L., and Fischer, P.J., 1972. Sediment transport on the Santa Barbara-Oxnard Shelf, Santa Barbara Channel, California. *In* Swift, D.J.P., Duane, D.B., and Pilkey, O.H. (Eds.), *Shelf Sediment Transport: Process and Pattern:* Stroudsburg, PA (Dowden, Hutchinson, and Ross), 307–331.

Dunbar, R.B., 1983. Stable isotope record of upwelling and climate from Santa Barbara Basin, California. *In* Thiede, J., and Suess, E. (Eds.), *Coastal Upwelling, its Sediment Record, Part B. Sedimentary Records of Ancient Coastal Upwelling:* New York (Plenum), 217–246.

Emmermann, R., Lauterjung, J., and Stroh, A., 1989. Das Lithostratigraphische Profil der KTB-Vorbohrung, bestimmt durch röntgenographische Phasenanalyse von Bohrkleinen. *KTB Rep.,* 89-3:152–164.

Fleischer, P., 1972. Mineralogy and sedimentation history, Santa Barbara Basin, California. *J. Sediment. Petrol.,* 42:49–58.

Heusser, L.E., 1978. Marine pollen in Santa Barbara, California: a 12,000 year record. *Geol. Soc. Am. Bull.,* 89:673–678.

Hickey, B.M., 1992. Circulation over the Santa Monica–San Pedro Basin and Shelf. *In* Small, L.F. (Ed.), *Progress in Oceanography:* Oxford (Pergamon Press), 30:37–115.

Hülsemann, J., and Emery, K.O., 1961. Stratification in recent sediments of Santa Barbara Basin as controlled by organisms and water character. *J. Geol.,* 69:279–290.

Janecek, T.R., and Rea, D.K., 1983. Eolian deposition in the northeast Pacific Ocean: Cenozoic history of atmospheric circulation. *Geol. Soc. Am. Bull.,* 94:730–738.

Kennedy, J.A., and Brassell, S.C., 1992. Molecular records of twentieth century El-Niño events in laminated sediments from the Santa Barbara basin. *Nature,* 357:62–64.

Kennett, J.P., Baldauf, J.G., et al., 1994. *Proc. ODP, Init. Repts.,* 146 (Pt. 2): College Station, TX (Ocean Drilling Program).

Lange, C.B., Burke, S.K., and Berger, W.H., 1990. Biological production off southern California is linked to climatic change. *Clim.Change,* 16:319–329.

Lange, H., 1982. Distribution of chlorite and kaolinite in eastern Atlantic sediments off North Africa. *Sedimentology,* 29:427–432.

Leinen, M., and Sarnthein, M., 1989. *Paleoclimatology and Paleometeorology: Modern and Past Patterns of Global Atmospheric Transport:* Doldrecht (Kluwer).

Müller, G., 1967. Methods in sedimentary petrology. *In* Von Engelhardt, W., Füchtbauer, H., and Müller, G. (Eds.), *Sedimentary Petrology* (Pt. 1): Stuttgart (Schweitzerbart'sche Verlagsbuchhandlung).

Pisias, N.G., 1978. Paleoceanography of the Santa Barbara Basin during the last 8000 years. *Quat. Res.,* 10:366–384.

Prospero, J.M., 1981. Eolian transport to the world ocean. *In* Emiliani, C. (Ed.), *The Sea* (Vol. 7): *The Oceanic Lithosphere:* New York (Wiley), 801–874.

Pye, K., 1987. *Aeolian Dust and Dust Deposits:* London (Academic Press).

Reimers, C.E., Lange, C.B., Tabak, M., and Bernhard, J.M., 1990. Seasonal spillover and varve formation in the Santa Barbara Basin, California. *Limnol. Oceanogr.,* 35:1577–1585.

Sarnthein, M., Tetzlaff, G., Koopmann, B., Wolter, K., and Pflaumann, U., 1981. Glacial and interglacial wind regimes over the eastern subtropical Atlantic and Northwest Africa. *Nature,* 293:193–196.

Schimmelmann, A., Lange, C.B., Berger, W.H., Simon, A., Burke, S.K., and Dunbar, R.B., 1992. Extreme climatic conditions recorded in Santa Barbara Basin laminated sediments: the 1835–1840 *Macoma* event. *Mar. Geol.,* 106:279–299.

Sholkovitz, E.R., and Gieskes, J.M., 1971. A physical-chemical study of the flushing of the Santa Barbara Basin. *Limnol. Oceanogr.,* 16:479–489.

Soutar, A., and Crill, P.A., 1977. Sedimentation and climatic patterns in the Santa Barbara Basin during the 19th and 20th centuries. *Geol. Soc. Am. Bull.,* 88:1161–1172.

Stein, R., Grobe, H., and Wahsner, M., 1994. Organic carbon, carbonate, and clay mineral distributions in eastern central Arctic Ocean surface sediments. *Mar. Geol.,* 119:269–285.

Stein, R., and Robert, C., 1986. Siliciclastic sediments at Sites 588, 590 and 591: Neogene and Paleogene evolution in the Southwest Pacific and Australian climate. *In* Kennett, J.P., von der Borch, C.C., et al., *Init. Repts. DSDP,* 90 (Part 2): Washington (U.S. Govt. Printing Office), 1437–1455.

Thornton, S.E., 1984. Basin model for hemipelagic sedimentation in a tectonically active continental margin: Santa Barbara Basin, California continental borderland. *In* Stow, D.A.V., and Piper, D.J.W. (Eds.), *Fine-grained Sediments.* Geol. Soc. Spec. Publ. London, 15:377–394.

van Andel, T.H., Heath, G.R., and Moore, T.C., Jr., 1975. Cenozoic history and paleoceanography of the central equatorial Pacific Ocean: a regional synthesis of Deep Sea Drilling Project data. *Mem.—Geol. Soc. Am.,* 143.

Date of initial receipt: 12 July 1994
Date of acceptance: 19 January 1995
Ms 146SR-273

Table 2. Summary table of Hole 893A data.

Core, section, interval (cm)	Depth (m)	Age (ka)	Sand	Silt	Clay	Smec	III	Kao	Chi	S/I	K/C	I/C	S/C	Quartz	Q426/FSP	Q334/FSP	KFS/PLAG	PLAG/FSP	Remarks
146-893A-																			
1H-1, 37–39	0.37	0.184	0.7	65.9	33.4	61	29	6	4	2.1	1.5	7.0	14.8	13.0	0.31	1.49	0.14	7.09	
1H-2, 37–39	1.85	1.012	1.6	61.8	36.6	61	27	7	5	2.2	1.5	5.7	12.8	14.4	0.40	1.30	0.00	>>	
1H-4, 26–28	4.76	2.754	0.9	62.7	36.4	58	28	7	6	2.1	1.3	4.9	10.1	15.4	0.26	1.10	0.45	2.24	
2H-1, 37–39	6.86	4.055	1.9	58.9	39.2	63	25	8	4	2.5	1.8	6.3	15.8	12.7	0.31	1.21	0.25	4.01	
2H-3, 37–39	9.79	5.910	0.7	65.6	33.6	59	30	6	5	2.0	1.2	5.9	11.7	12.6	0.23	1.27	0.38	2.62	
2H-5, 37–39	12.52	7.667	0.7	62.8	36.5	58	30	7	6	1.9	1.2	5.3	10.2	12.7	0.35	1.15	0.45	2.20	
2H-7, 53–55	15.44	9.575	0.0	68.3	31.7	44	44	5	7	1.0	0.8	6.5	6.5	21.7	0.30	1.30	0.43	2.32	Gray bed
3H-2, 38–40	17.85	11.164	0.3	60.0	39.6	60	26	7	6	2.3	1.1	4.1	9.3	22.0	0.35	1.29	0.32	3.16	
3H-6, 35–37	23.51	14.946	1.3	60.3	38.4	57	33	5	5	1.7	1.2	7.2	12.2	21.1	0.43	1.36	0.20	4.96	
4H-3, 37–39	28.53	18.346	2.8	67.3	29.9	63	26	6	5	2.4	1.4	5.6	13.6	20.4	0.29	1.17	0.08	13.05	
4H-5, 38–40	31.20	20.169	0.9	34.3	64.9	54	33	7	6	1.7	1.2	5.3	8.8	19.2	0.31	1.43	0.08	12.00	
5H-1, 37–39	35.37	23.035	1.0	60.5	38.6	55	30	8	7	1.8	1.1	4.5	8.2	21.5	0.28	1.32	0.28	3.56	
5H-4, 37–39	39.36	25.796	1.2	63.9	34.9	58	29	7	6	2.0	1.3	5.0	9.9	18.9	0.23	1.01	0.08	12.86	
6H-1, 37–39	44.80	30.069	6.1	66.2	27.7	55	32	7	6	1.7	1.2	5.3	9.2	23.0	0.22	1.25	0.17	5.98	
6H-4, 37–39	48.61	32.810	1.4	72.1	26.5	53	34	7	6	1.5	1.1	5.4	8.4	21.5	0.28	1.31	0.29	3.41	
7H-2, 37–39	54.42	36.991	5.2	65.2	29.7	52	34	8	6	1.5	1.4	6.2	9.5	18.0	0.40	1.24	0.32	3.13	
7H-5, 109–110	58.65	40.034	86.2	11.9	1.9	43	39	9	9	1.1	1.0	4.3	4.7	54.7	0.32	1.93	0.70	1.42	Sand bed
7H-6, 21–22	59.22	40.444	86.7	11.1	2.2	40	41	10	9	1.0	1.1	4.7	4.6	50.9	0.31	1.63	0.81	1.23	Sand bed
7H-6, 37–39	59.38	40.560	25.8	47.9	26.2	56	30	8	7	1.9	1.2	4.4	8.3	20.6	0.26	1.41	0.29	3.44	Sandy silt
8H-3, 35–37	65.36	44.862	4.9	52.1	43.0	68	26	5	2	2.6	2.1	11.8	31.0	10.0	0.29	1.22	0.10	10.35	
8H-6, 37–39	69.05	47.517	37.9	42.1	20.0	56	31	7	6	1.8	1.2	5.0	9.1	43.7	0.23	1.29	0.89	1.13	Sandy silt
9H-2, 25–27	74.50	51.514	0.1	60.0	39.9	61	30	6	3	2.1	1.8	8.6	17.8	15.2					
9H-2, 36–38	74.61	51.607	0.7	62.6	36.7	55	31	8	6	1.8	1.2	5.0	8.7	13.8	0.24	1.18	0.08	13.09	
9H-5, 36–38	78.49	54.880	0.8	61.6	37.6	55	32	7	7	1.7	1.1	4.8	8.3	21.7	0.36	1.33	0.26	3.92	
10H-2, 37–39	84.23	59.720	2.0	66.6	31.4	56	31	7	6	1.8	1.1	4.8	8.6	20.1	0.30	1.37	0.25	4.04	
10H-6, 37–39	90.23	64.781	0.6	63.1	36.3	45	38	9	8	1.2	1.3	5.0	6.0	22.5	0.26	1.27	0.14	7.23	
11H-3, 37–39	95.26	70.097	1.6	61.0	37.5	48	37	9	6	1.3	1.6	6.4	8.4	20.0	0.36	1.48	0.17	5.97	
11H-6, 37–39	98.78	73.858	0.4	67.5	32.1	49	38	9	5	1.3	1.8	8.0	10.2	17.3	0.34	1.42	0.05	21.60	
12H-3, 37–39	104.63	80.109	0.4	37.5	62.1	52	33	8	7	1.6	1.3	5.0	7.9	18.8	0.32	1.20	0.37	2.67	
12H-7, 37–39	109.32	85.120	30.0	47.9	22.1	51	37	7	6	1.4	1.2	6.4	8.9	25.6	0.27	1.38	0.30	3.33	Sandy silt
13H-4, 23–25	113.83	89.939	0.3	61.7	38.0	56	32	8	4	1.7	2.2	8.7	15.3	18.0	0.25	1.34	0.27	3.70	
13H-8, 34–36	119.89	93.778	2.0	58.1	39.8	49	38	9	5	1.3	1.9	8.3	10.7	15.9	0.39	1.38	0.22	4.65	
14H-4, 37–39	125.42	99.687	1.3	61.4	37.3	47	40	8	4	1.2	2.0	9.6	11.1	17.7	0.36	1.54	0.05	19.13	
14H-9, 37–39	130.24	104.837	1.0	63.6	35.4	44	40	10	7	1.1	1.5	6.1	6.7	16.9	0.27	1.19	0.38	2.63	
15H-4, 37–39	134.63	109.528	1.4	64.5	34.1	49	36	9	6	1.4	1.5	5.9	8.1	24.5	0.21	1.03	0.42	2.38	
16H-1, 37–39	139.75	114.999	1.6	62.4	36.0	44	40	10	6	1.1	1.5	6.5	7.1	25.2	0.33	1.27	0.15	6.55	
16H-4, 37–39	144.16	119.362	0.1	50.9	48.9	57	32	7	4	1.8	2.0	9.0	16.2	19.7	0.38	1.52	0.09	11.33	
16H-7, 37–39	148.70	123.145	0.5	62.3	37.2	52	34	8	6	1.6	1.3	5.5	8.5	16.8	0.29	1.01	0.60	1.68	
17H-5, 37–39	155.48	126.344	1.0	57.6	41.4	56	30	7	6	1.9	1.2	4.8	9.0	15.3	0.35	1.32	0.06	15.50	
18H-2, 36–38	160.26	130.053	0.3	59.4	40.3	55	33	7	5	1.7	1.3	6.3	10.6	14.3	0.33	1.39	0.29	3.47	
18H-5, 34–36	164.77	134.115	0.6	63.4	36.0	52	33	8	7	1.6	1.1	4.9	7.7	20.2	0.31	1.37	0.09	11.04	
19H-2, 37–39	169.79	138.636	1.3	62.2	36.6	57	30	7	6	1.9	1.1	4.9	9.3	21.7	0.34	1.38	0.12	8.49	
19H-5, 37–39	174.25	142.652	0.4	43.5	56.1	57	31	7	5	1.8	1.4	5.7	10.5	17.9	0.29	1.45	0.23	4.35	
20H-2, 37–39	179.21	147.119	1.1	60.7	38.3	55	32	7	6	1.7	1.2	5.0	8.7	24.8	0.30	1.62	0.13	7.72	
20H-6, 37–39	185.12	152.442	2.5	62.0	35.5	52	35	8	5	1.5	1.5	6.7	9.8	18.5	0.28	1.30	0.16	6.35	
21H-3, 37–39	189.92	156.765	0.8	64.0	35.2	49	37	8	5	1.3	1.5	6.8	9.1	23.1	0.35	1.61	0.17	5.72	
21H-6, 37–39	194.50	160.890	0.7	63.2	36.1	53	32	8	6	1.6	1.3	5.1	8.3	18.6	0.34	1.82	0.20	4.88	

Notes: Sample number; void-corrected depth (after Merrill and Rack, 1994); age (ka) based on AMS ^{14}C chronology and oxygen-stable isotope stratigraphy (after Ingram and Kennett, this volume); sand-clay concentrations (% of the bulk sediment); smectite, illite, kaolinite, and chlorite concentrations (in % of the clay minerals); smectite/illite, kallinite/chlorite, illite/chlorite, and smectite/chlorite ratios; quartz concentration (% of the bulk sediment); quartz$_{4.26Å}$/feldspar, quartz$_{3.34Å}$/feldspar, and plagioclase/kalifeldspar ratios.

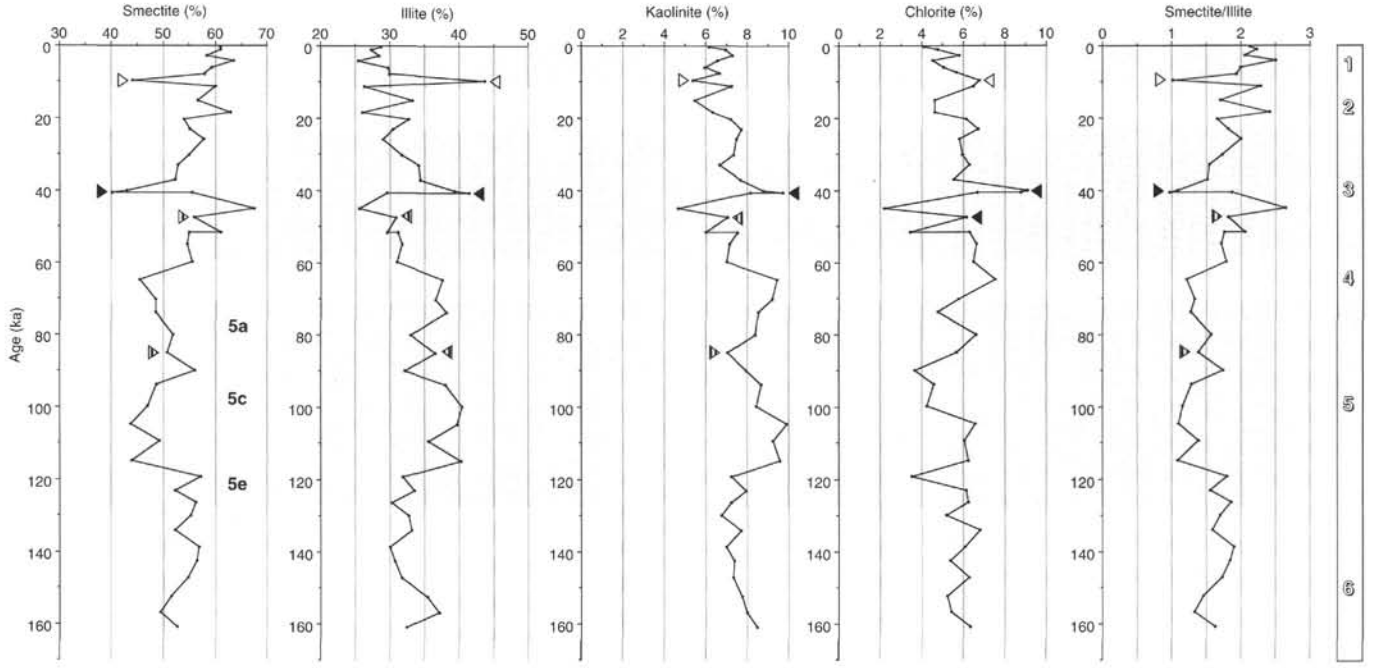

Figure 5. Clay-mineral distribution and smectite/illite ratio vs. age at Site 893. Open triangle marks gray-bed sample, black triangle marks sand-bed sample, and hatched triangles mark samples from sandy-silt intervals.

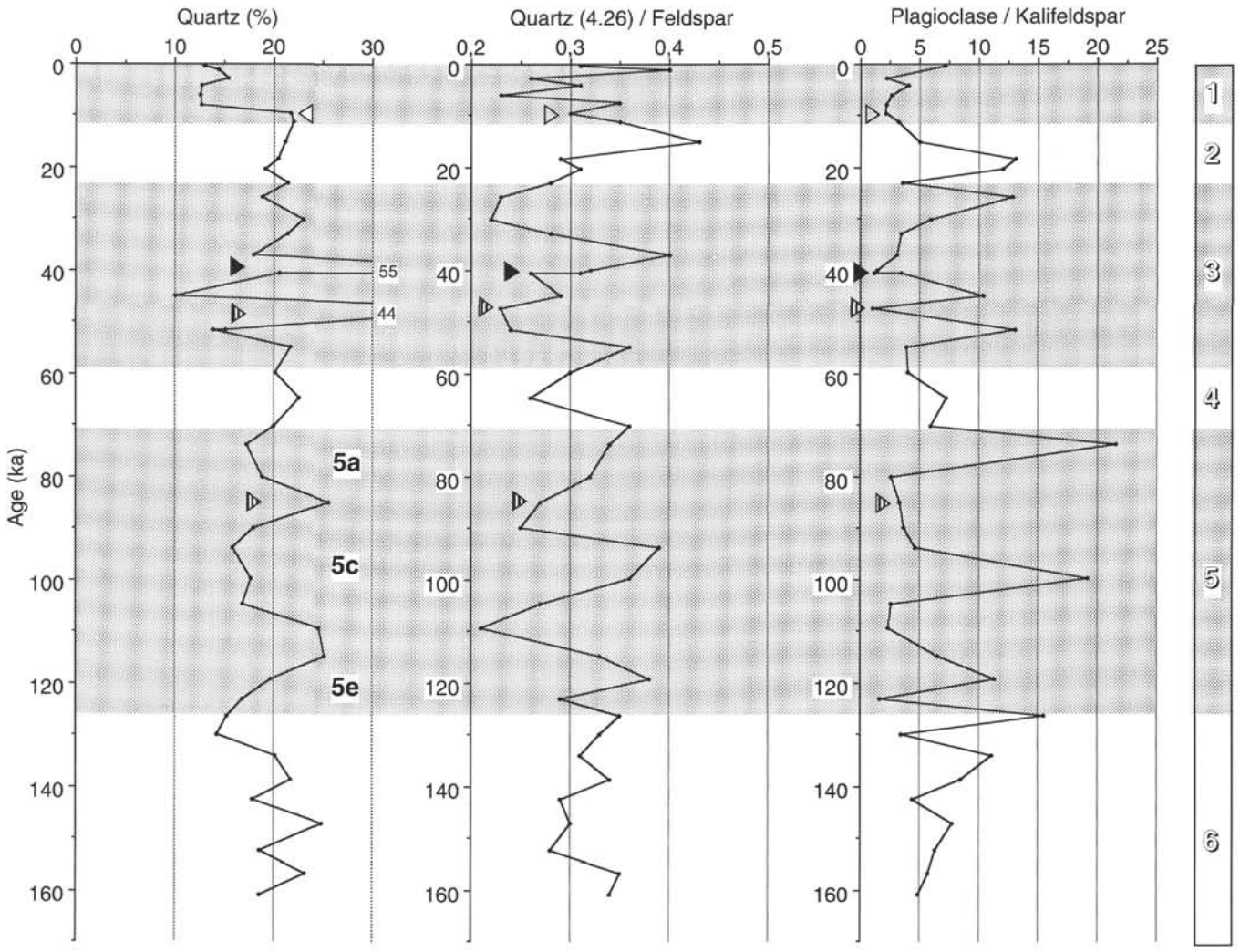

Figure 6. Quartz concentrations and quartz/feldspar and plagioclase/kalifeldspar ratios vs. age. Open triangle marks gray-bed sample, black triangle marks sand-bed sample, and hatched triangles mark samples from sandy-silt intervals.

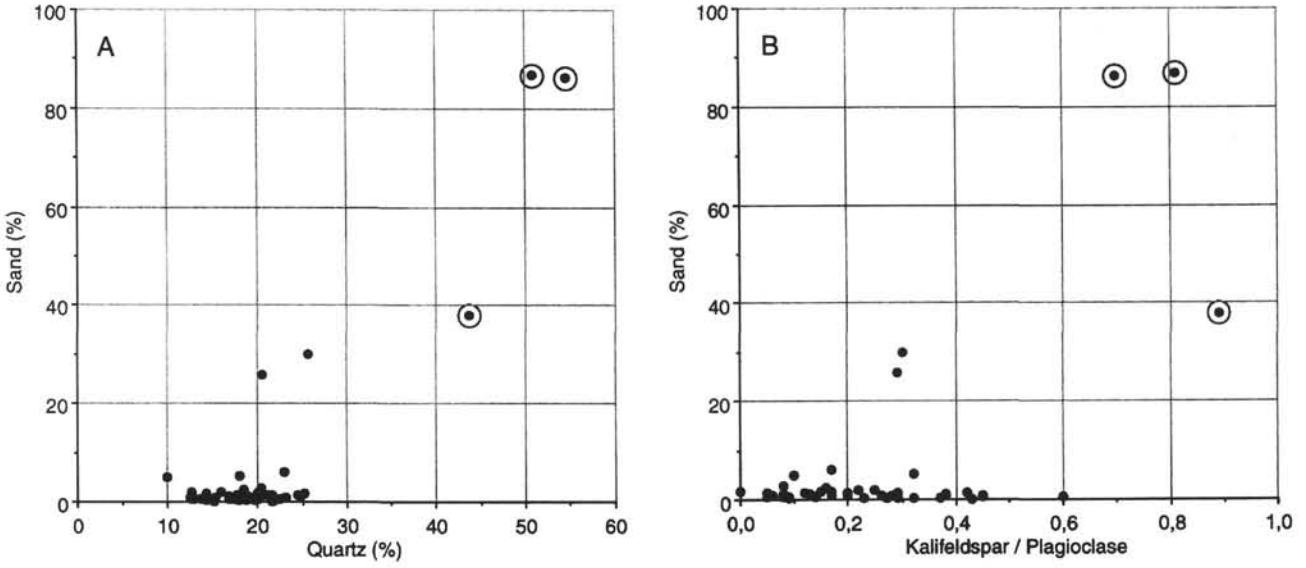

Figure 7. **A.** Quartz vs. sand diagram. **B.** Kalifeldspar/plagioclase vs. sand diagram. Circled data points are from sand beds and sandy silts.

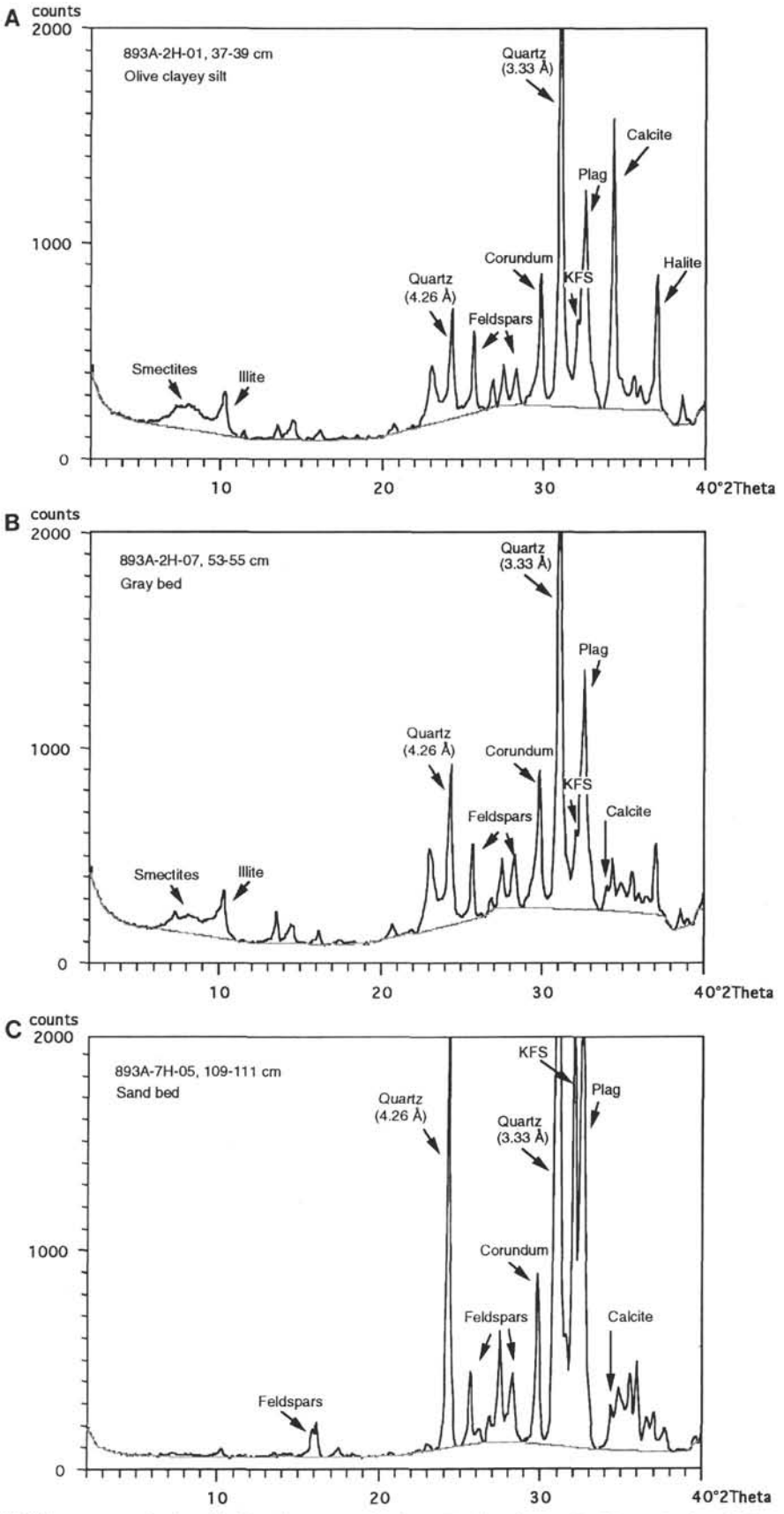

Figure 8. Diffractograms of selected bulk sediment samples from **(A)** olive clayey silt, **(B)** gray bed, and **(C)** sand bed.

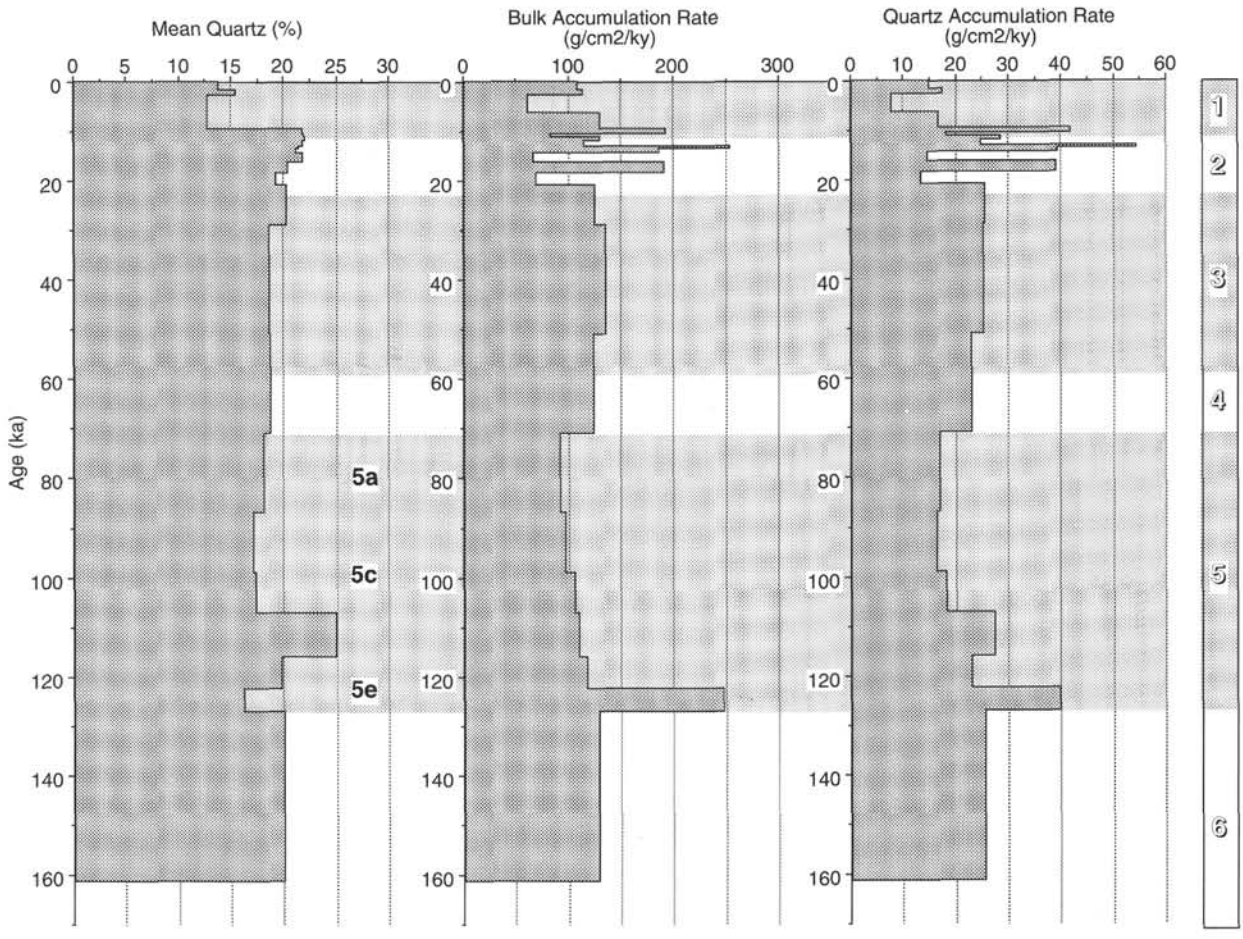

Figure 9. Mean quartz contents (%), bulk accumulation rates, and quartz accumulation rates (for data source see Table 3). When interpreting these records one has to consider the much higher time resolution of accumulation rates in the upper part of the records in comparison to the lower part.

Table 3. Sedimentation rates, dry density, bulk accumulation rate, mean quartz concentrations, and quartz accumulation rates at Site 893.

Depth (mbsf)	Age (years)	SR (cm/ky)	DD (g/cm^3)	Bulk AccRate ($g/cm^2/ky$)	Mean Quartz (%)	Quartz AccRates ($g/cm^2/ky$)
0	0					
		217	0.5	108	13.7	14.8
3.62	1,670					
		185	0.61	113	15.4	17.4
5.67	2,780					
		89	0.69	61	12.7	7.7
8.71	6,190					
		167	0.78	130	12.7	16.5
13.97	9,340					
		267	0.72	192	21.7	41.7
16.99	10,470					
		103	0.8	82	21.9*	18
17.6	11,060					
		151	0.86	130	22	28.6
18.75	11,820					
		142	0.8	114	21.7*	24.7
20.39	12,971					
		333	0.76	253	21.4*	54.1
21.94	13,436					
		224	0.83	186	21.1	39.2
24.12	14,411					
		79	0.84	66	21.8*	14.4
25.58	16,267					
		203	0.94	191	20.4	39
29.61	18,254					
		75	0.92	69	19.2	13.2
31.52	20,792					
		144	0.87	125	20.2	25.3
43.17	28,896					
		139	0.97	135	18.6	25.1
73.89	51,000					
		119	1.03	123	18.9	23.2
96.1	71,000					
	5a	98	0.94	92	18.1	16.7
	5b	98	0.98	96	17	16.3
	5c	98	1.07	105	17.3	18.1
	5d	98	1.11	109	24.9	27.1
140.69	116,000					
		103	1.14	117	19.7	23.1
147.46	122,560					
		212	1.16	246	16.1	39.6
156.87	127,000					
		111	1.15	128	19.9	25.5
195	161,340					

Notes: * = interpolated values; sedimentation rate data from Ingram and Kennett (this volume); dry density data from Rack (this volume).